Connecting the Elementary Reaction Pathways of Criegee Intermediates to the Chemical Erosion of Squalene Interfaces during Ozonolysis

Nadja Heine, Frances A. Houle,* and Kevin R. Wilson*

Chemical Sciences Division, Lawrence Berkeley National Laboratory, Berkeley, California 94720, United States

*E-mail: krwilson@lbl.gov, fahoule@lbl.gov

Criegee Intermediates (CI), formed in alkene ozonolysis, are central for controlling the multiphase chemistry of organic molecules in both indoor and outdoor environments. Here we examine the heterogeneous ozonolysis of squalene, a key species in indoor air chemistry. Aerosol mass spectrometry is used to investigate how the ozone (O_3) concentration, relative humidity (RH) and particle size control reaction rates and mechanisms. Although the reaction rate is found to be independent of RH, the reaction products and particle size depend upon H_2O. Under dry conditions (RH =3%) the reaction produces high molecular weight secondary ozonides (SOZ), which are known skin irritants, and a modest change in particle size. Increasing the RH reduces the aerosol size by 30%, while producing mainly volatile aldehyde products; increasing potential respiratory exposure. Chemical kinetics simulations link the elementary reactions steps of CI to the observed kinetics, product distributions and changes in particle size. The simulations reveal that ozonolysis occurs near the surface, and is O_3 transport limited. The observed secondary ozonides are consistent with the formation of mainly secondary CI, in contrast to gas phase ozonolysis mechanisms.

Introduction

Accurately predicting molecular weight growth and decomposition of products formed during the oxidation of organic material requires understanding how the reaction pathways of transient intermediates such as free radicals or Criegee intermediates (CI) generate multiphase reaction products. CI produced from the ozonolysis of terpenes build molecular weight by forming condensable vapors and organic aerosol in the troposphere.[1, 2] On indoor surfaces, thin films of skin lipids (e.g. squalene, unsaturated acids) contain reactive C=C bonds that are oxidized by ozone, producing both gas and condensed phase reaction products.[3-6] Here we examine the ozonolysis of liquid squalene aerosol in an effort to elucidate how CI reaction steps control product formation on model indoor interfaces.

Understanding and improving indoor air quality is important,[7] especially as people spend a significant fraction of their daily life inside (over 90%).[8] In contrast to the extensive research devoted to the health effects of outdoor air pollution, significantly less is known about the impact of indoor air quality. A prevalent indoor oxidant, ozone (O_3), readily reacts with unsaturated organic molecules in the gas phase and on surfaces such as skin.[4, 9] Reactions with O_3 can produce harmful substances and increase the quantity of volatile organic compounds (VOC), with associated impacts on the respiratory system. High indoor concentrations of VOCs are mainly the consequence of large surface areas and diverse sources, such as cleaning products, cooking and occupants, which are concentrated in small enclosures often with limited air exchange.[10, 11]

Skin lipids on indoor surfaces are typically emitted via desquamation from skin and hair, or from clothes[3] at a rate of 30–90 mg of skin flakes/h.[12] Squalene (Sqe) represents one of the most abundant unsaturated constituents of the human sebum (≤12%).[13] Its six double bonds make Sqe

highly reactive towards ozone. As a result, significant effort has been devoted to identifying the volatile and semi-volatile oxidation products formed in Sqe ozonolysis (e.g. in chamber studies,[5] an aircraft cabin,[14] class rooms[15] and office environments[16]). A study by Lakey *et al.* explored how semi-volatile and low volatile reaction products diffuse through skin layers and enter the bloodstream.[17] In laboratory experiments, Zhou *et al.* quantified some of the condensed phase products of Sqe ozonolysis and found evidence that the relative humidity (RH) played a large role in the reaction mechanism.[6] These studies clearly show that distribution of products remaining on the skin versus those that are in the gas phase can vary greatly (along with potential health effects) and will depend upon the changes in the indoor environment (RH, O_3 concentration [O_3], air exchange rate, etc.).

The objective of this study is to develop a quantitative description of reactive uptake of ozone onto Sqe gas-liquid interfaces. Here the squalene surface is in the form of an aerosol, such as would occur from cooking with oil,[18] rather than a film on an indoor surface (e.g. skin, window or tabletop). Submicron particles are used to take full advantage of advanced aerosol mass spectrometry and mobility sizing techniques to measure the real-time evolution of reactants and products, enabling closer examination of how their formation connects to the chemical erosion of the interface. Our objective is to use these measurements to develop a predictive, quantitative kinetic model of the multiphase chemistry that in turn can be adapted to any sample configuration (aerosol or monolayer). We focus on how the elementary reaction pathways of CI depend upon relative humidity and ozone concentration, and how these pathways produce both gas and condensed phase reaction products. Furthermore, we explore the origin of the large discrepancy in reported uptake coefficients which range from 10^{-3} to 10^{-6} [6, 19-23], and discuss impacts of the reactions and conditions on indoor air quality and health.

Methods

Experiment. The heterogeneous reaction of ozone with Sqe is measured in an aerosol flowtube reactor. Polydisperse Sqe particles with a log-normal size distribution with a mean surface-weighted diameter of ~250 ± 40 nm are generated from heated liquid Sqe (T = 145°C) in a tube furnace. Particles are entrained in a 300 sccm flow of N_2 and passed through an activated charcoal denuder in order to remove gas phase components. For monodisperse measurements, the aerosol flow is size-selected with a TSI Electrostatic Classifier (3080L). The aerosol flow is then mixed with 10% O_2, and variable amounts of dry and humidified N_2 (RH) as well as O_3 (0-4 ppm), yielding a total flowrate of 1 lpm. The gas/particle mix is introduced into the flow reactor with a residence time of 37 s.[24] Ozone is produced by a corona discharge generator and measured with an ozone monitor (2B Technology 106-L). The flow exiting the reactor is analyzed by a second TSI Electrostatic Classifier coupled with a butanol TSI Condensation Particle Counter (3772) and a homebuilt vacuum ultraviolet aerosol mass spectrometer (VUV-AMS). For analysis of the heterogeneous kinetics and product formation, the aerosol is thermally vaporized followed by photoionization using 10.2 eV VUV radiation at the Chemical Dynamics Beamline (Advanced Light Source, Berkeley CA.)[25] Using mass spectral intensities to determine reaction product populations is difficult due to uncertainties in cross sections and ion fragmentation. Thus, comparisons between model and measured reaction products are expected to capture only the product kinetic evolution vs. ozone exposure and RH rather than absolute product abundance.

The main experimental observables are the reactive decay of squalene exposed to ozone as a function of particle size and relative humidity, the formation kinetics of the major reaction products, and changes in particle size. These form the data set against which the mechanistic model description of the heterogeneous reaction, described below, is developed and evaluated.

Simulation methodology. Kinetic modeling of the experimental results is conducted using Kinetiscope,[26] which uses stochastic algorithms to propagate sets of elementary reactions. As described in previous publications on heterogeneous aerosol chemistry,[27-29] the aerosol is represented as a single instantaneously mixed volume, which is a valid assumption for reactions on particles that are well-mixed relative to the heterogeneous gas-aerosol collision frequency.[30] To properly account for surface to volume scaling when the aerosol volume changes dynamically during the reaction, the aerosol is represented by a 1 nm x 1 nm x R/3 nm rectangular volume where R is the measured experimental aerosol radius. [29] O_3 adsorption occurs only in a 1 nm thick portion of the 1 nm^2 surface region, rather than throughout the entire volume of the aerosol. Within this subvolume it is assumed that each Sqe molecule provides 1 adsorption site for gaseous O_3, and this number of sites is held constant as the reaction proceeds. Because the single compartment model used in this work involves surface reactions as well as bulk reactions, all reaction rates are expressed in per unit volume form, since it is not possible to mix 2- and 3- dimensional kinetics using the stochastic algorithm in its current form. Description of a surface reaction in terms of a volume is not a drastic assumption for liquids and soft solids since the outer surfaces are diffuse.

Construction of the reaction mechanism. As will be detailed below, the model incorporates three main processes: **1)** ozone adsorption, **2)** condensed phase reactions within the particle, and **3)** evaporation of volatile reaction products.

Ozone adsorption kinetics. The pseudo-first order rate constant of ozone adsorption on the aerosol surface is,

$$[O_3] \cdot Z \cdot S, \quad (1)$$

where [O_3] is the average gas phase ozone concentration in the experiment, S is the sticking coefficient, and Z is the ozone collision frequency, given by: $\sigma \cdot \nu$, with σ as collision cross section (1 x 1 nm^2), and v the mean speed of ozone (390.29 m/s). A value of $S = 1.96 \cdot 10^{-4}$ was measured previously for ozone sticking on submicron carbonaceous particles.[31] To achieve model agreement with the experimental data a slightly smaller value is needed ($1.8 \cdot 10^{-4}$), which appears reasonable given our estimated error in previous experiments and the expected differences between sticking on the squalene surface vs. a carbonaceous particle. This single value of S, originally obtained using a single data set was found to accurately represent the global data set (i.e. squalene decay kinetics vs. particle size). As discussed below, we evaluated the possibility that the ozonolysis reaction occurs through the entire volume of the particle. In this case, the rate would not be governed by the surface collision frequency but rather by the Henry's Law solubility of O_3.

Construction of the ozonolysis reaction scheme. The ozonolysis mechanism of Sqe used for the simulations was previously reported, and is shown schematically in Figure 1.[6, 20, 32] The rate constants are shown in Table 1. It is preferable to use condensed phase rate coefficients but unfortunately for many reactions studied here they are not available. For the model gas-phase rate constants are used as reasonable starting points since energy barriers for many reactions should be similar in both phases. The mechanism has three main parts: 1) the formation of the primary ozonide (POZ, **R1**), followed by 2) dissociation of the POZ into a ketone or aldehyde and CI (**R1**), and 3) subsequent reactions of the CI (**R2-R6**).

Formation of the POZ is multigenerational, since a single squalene molecule (with six double bonds) can undergo repeated **R1** reactions with O_3. The POZ is transient, and the rate coefficient is for a composite step that forms either a primary or a secondary CI. For simplicity, we use the same rate coefficients for each generation in the reaction mechanism. We assume that

each double bond is equally reactive, and the literature rate coefficient for the overall reaction (e.g. Sqe + O_3) is divided by the number of double bonds (the statistical factor) to obtain the rate coefficient for each. This appears to be a reasonable approximation for this study, which is mainly focused on the formation pathways of the first and second generation reaction products. Reactions at each unique double bond location are tracked explicitly since the reaction products and the CI that are formed in step **R1** depend upon where the reaction with ozone occurs. Additional model details can be found in the Supporting Information (SI).

Once formed, the main reaction pathways of CI are: (**R2**) reaction with water to form carbonyls, (**R3**) reaction with carbonyls to form secondary ozonides (SOZ), (**R4**) unimolecular rearrangement, and (**R6**) reaction with ozone to form a carbonyl.

As seen in the experiments described below, water plays a central role both in the specific products that remain in the particle and those that are released to the gas phase (inferred via mass loss from the aerosol). **R2** and **R3** are competitive sinks for the CI, depending directly and indirectly on water, and producing the observed carbonyl and SOZ products. The rate coefficient used for **R2** is taken from a previous gas phase measurement of CI + H_2O.[33] **R2** is assumed to occur in the bulk of the aerosol so its overall rate is also governed by RH in the reaction and by the Henrys law constant for H_2O in an organic solvent (Table 1).

To our knowledge, the only coefficients for **R3** (k_{CO}) are for the simplest gas phase CI (formaldehyde oxide) reacting with either acetone (k_{CO}=2.3±0.3·10^{-13} cm^3 $molec.^{-1}$ s^{-1}) or acetaldehyde (k_{CO} =9.5±0.7·10^{-13} cm^3 $molec.^{-1}$ s^{-1}).[34] Unfortunately, these gas phase CI + carbonyl rate coefficients produced simulation results that are not in agreement with observations, suggesting that entropic factors are significant. Specifically, **R3** (i.e. CI + carbonyl) was predicted

to be the dominant sink for the CI, producing large quantities of SOZ at RH = 60% and substantial aerosol growth under dry conditions. Neither is consistent with experimental measurement of the products and aerosol size. Therefore, we treated k_{CO} as the only adjustable parameter in the model. An estimate for it was made by varying k_{CO} until the RH dependence of the carbonyl and SOZ product concentrations could be reasonably reproduced. k_{CO} was optimized at $1.33 \cdot 10^{-18}$ cm^3 molec.$^{-1}$ s^{-1} for species that form and immediately react within the same solvent cage, and $6.7 \cdot 10^{-19}$ cm^3 molec.$^{-1}$ s^{-1} for all other combinations. That these values are so small relative to the gas phase is not surprising since the cage effect on recombination rate coefficients is well known. The factor of ~ 2 difference between the intra-cage and extra-cage reaction coefficients has been observed in other systems. For example the recombination rate coefficient of newly formed acetyl peroxide radicals in octadecane is approximately double the value obtained when one of the radical species leaves the solvent cage and reacts later.[35]

The rate constant for CI + O_3 (**R6**) is taken from Veerecken *et al.* and is based on coupled cluster calculations in combination with theoretical kinetic predictions of the rate coefficients.[36]

The unimolecular reactions of the CI include isomerization to acids (**R4a**) or α-hydroxyketones (**R4b**), and 1,4 H-shifts (**R5**). The rate coefficient for isomerization (**R4**) is assumed to be equal to that for the decomposition of CIs in the gas phase. In the gas phase, an excited acid intermediate forms and rapidly eliminates CO_2, forming a new C=C bond that can react further with O_3. In the condensed phase, however, this intermediate is collisionally stabilized to form an acid product. Literature values for CI isomerization range from 1.5 to 305 s^{-1}.[37, 38] Here, 5 s^{-1} is used for the simulations. A sensitivity test (Figure S1) shows that this isomerization rate is too slow to be kinetically competitive with the bimolecular reaction **R2** when the RH is elevated. The hydride shift reaction **R5** has been observed in the gas phase[37, 39] and its importance in the

condensed phase reactions is uncertain as will be discussed below in the context of the experimentally observed reaction products.

Evaporation. Evaporation is considered to be an irreversible desorption step from the surface of the particle. Repartitioning of gas phase products that have undergone further reaction are neglected, since C=C bond scission favored under wet conditions will form products that remain in the gas phase. Evaporation rate constants, k_{evap}, were calculated using the formulation reported in Wiegel *et al.*[27, 40] (see also Equation (2) in the SI), and depend upon the geometry of the particle and the saturation vapor pressure (p_{sat}) of the corresponding species.[41] If available, measured vapor pressures are used. If they are not, p_{sat} are computed (see Table S1) using group contribution methods (i.e. EVAPORATION),[42] and are reasonably consistent with previous estimates employing a different software package.[17] Uncertainties in the estimated vapor pressures are evaluated as shown in Figure S2. The aerosol volume is obtained from the simulation compartment volume, which is calculated from the instantaneous populations and densities of all condensed phase species. As species evaporate from the aerosol, the volume dynamically decreases, leading to increases in concentrations and reaction rates. An increase or decrease of k_{evap} by a factor of 10 has a negligible effect on the predicted reaction kinetics and volume change of the particle.

Results and Discussion

In this section we examine the experimental and simulated decay of Sqe to elucidate where the reaction occurs (heterogeneous vs. bulk) and whether ozone uptake is transport or reaction limited. We identify the major reaction products, their kinetic evolution and RH dependence. This provides the basis for understanding which key reaction pathways are active and why. Finally, we discuss implications of the results for indoor air chemistry.

Heterogeneous kinetics of squalene ozonolysis. Shown in Figure 2a is the measured decay of Sqe as a function of ozone exposure and RH, determined using the parent molecular ion (at *m/z* =410) in the aerosol mass spectrum (Figure 3) as a function of ozone exposure. The observed decays are nearly exponential and independent of RH. Also shown in Figure 2a is the simulated decay of Sqe at all four RHs, which agree with experiment and depend only on the average ozone concentration of the particular experiment. Although recent work has shown compelling evidence that O_3 reacts within the first 1-2 nm of a squalene surface,[19] we have nevertheless considered two different simulation scenarios to examine the (*i*) surface vs (*ii*) bulk reactivity of O_3.

As described earlier, two elementary steps are used to describe the reaction of O_3 with Sqe. In the simulation, ozone first adsorbs to the squalene surface (described by Equation (1)) after which it reacts with Sqe (**R1**, Figure 1). There are two previously reported values for the rate coefficient for the Sqe + O_3 reaction that differ by a factor of 100: one for Sqe + O_3 in a dilute solution of chloroform ($1.25 \cdot 10^{-15}$ cm^3 s^{-1})[43] and the other is estimated from O_3 transmission measurements through a thin squalene coating ($1.21 \cdot 10^{-13}$ cm^3 s^{-1}).[19] To determine which is correct, we have compared experimental values for the phenomenological rate coefficients (k_{obs}) calculated from an exponential fit of the measured decay of Sqe (as a function of aerosol size) to those for simulated decays as shown in Figure 2c at RH=3%. The model used a Sqe + O_3 rate coefficient of $1.25 \cdot 10^{-15}$ cm^3 s^{-1} (k_1, Scenario 1) or $1.21 \cdot 10^{-13}$ cm^3 s^{-1} (k_2, Scenario 2). For both simulation and experiment the aerosol size ranged from 71 to 530 nm. For diameters between 200 and 500 nm both model Scenarios predict nearly identical results, despite the factor of 100 difference in Sqe + O_3 rate coefficient. It is only for experiments on smaller particles that a difference between Scenario 1 and 2 appears, indicating that neither Scenario completely reproduces the entire data set. It is interesting to note that although there is an increase at smaller

sizes, k_{obs} does not strictly follow the inverse radius scaling expected for a reaction localized at the surface, suggesting a more complex relationship. It appears that the observed decay of squalene is not simply controlled by the Sqe + O_3 rate coefficient but rather that it is the adsorption rate of O_3 on the surface that is limiting (i.e. gas phase transport limited).

We examined the possibility that the O_3 + Sqe reaction occurs within the volume of the aerosol rather than at its surface. In this case [O_3] would be governed by its Henry's law constant rather than a transient surface population. Details of this kinetic description are given in the SI. Figure 2b compares the experimental Sqe decay with the simulated surface and bulk reaction predictions. Both bulk Scenarios predict a much slower consumption rate of Sqe than is observed by experiment or in the surface Scenarios. This result further confirms the previously determined short reactive-diffusive lengths (~1 nm) of ozone in Sqe.[19]

Reaction products. Reaction products are formed according to the mechanism in Figure 1. The exact distribution of products is governed by the location (i.e., which C=C bond) of the initial ozone attack. Squalene has six double bonds, and because of symmetry there are only three unique reactive sites for the formation and decomposition of the POZ. If the POZ decomposes into a primary CI (p-CI, **R1** Figure 1) then its co-product will be a ketone. Thus there are three unique p-CI that could form with carbon lengths of C_{27}, C_{22} and C_{17} as shown in Figure S3. The ketone coproducts of these CI have corresponding carbon numbers of C_3 (acetone), C_8 and C_{13}, respectively. Alternatively, the POZ could form a secondary CI (s-CI) and an aldehyde. In this case, reaction at the three double bonds will produce smaller s-CI with carbon lengths of C_3, C_8 and C_{13}. The aldehyde co-products have corresponding carbon numbers of C_{27}, C_{22}, and C_{17}, respectively (see Figure S4). Thus, the chemistry of squalene will be controlled in large part by

how the POZ decomposes to form p- and/or s-CI, with the corresponding small carbon number ketones and/or larger molecular weight aldehydes.

Figure 3 shows aerosol mass spectra (MS) of the ozonolysis products as function of RH. These spectra are all recorded after approximately 50% of the Sqe in the aerosol has been consumed. Peaks corresponding to pure squalene have been removed by subtracting the unreacted squalene mass spectrum. Analysis of the lower mass range (m/z <150) in Figure 3 is challenging, since it is difficult to distinguish small molecular weight reaction products from fragment ions produced by dissociative photoionization of larger species. Products in this mass region will most likely evaporate from the aerosol, and thus be underrepresented. Thus, we focus on explaining the kinetics of the main SOZ and aldehyde products.

The product distribution is a sensitive function of relative humidity as expected from the mechanism in Figure 1. The spectrum recorded at the lowest humidity (3% RH, Figure 3a) shows a series of peaks at masses larger than unreacted squalene ($m/z = 410$), which can be easily assigned to SOZs. The highest intensity SOZ appears at $m/z = 458$ and is assigned to the C_{30} SOZ. The other SOZ's are observed at m/z = 322.25, 390.31, 526.43 and 594.50 and are assigned to C_{20}, C_{25}, C_{35} and C_{40} SOZ's, respectively.

The observed pattern of SOZ's (C_{20}, C_{25}, C_{30}, C_{35}, C_{40}) reveals key details about the reaction mechanism. Most of the C_{30} SOZ likely forms inside a solvent cage by the reaction of a CI with its coproduct carbonyl; both originating from a common POZ. This reaction requires a simple molecular rotation of the CI relative to the carbonyl co-product. If the CI and its carbonyl co-product escape the solvent cage before reacting, then a much larger array of possible SOZ's can form. As shown in Figure S5 and Table S2, there are 15 possible SOZ's that could form from all of the potential reactive combinations of p- and s-CI with ketones and aldehydes. These are C_6,

C_{11}, C_{16}, C_{20}, C_{21}, C_{25}, C_{26}, C_{30}, C_{34}, C_{35}, C_{39}, C_{40}, C_{44}, C_{49}, and C_{54}. Only a small subset of these SOZ possibilities are observed in the experiment; C_{20}, C_{25}, C_{30}, C_{35}, and C_{40}. This can only be explained if the POZ that is formed decomposes exclusively into either a p-CI and a ketone or a s-CI and an aldehyde as shown in Figure S6 and Table S2. Analysis of the changes in aerosol volume indicate that Sqe ozonolysis forms mainly s-CI and aldehydes as will be demonstrated below.

As the relative humidity increases, the SOZ products decrease, vanishing completely at RH = 60%. Since SOZ's (**R3,** Figure 1) are formed by the reaction of the CI with a carbonyl, this indicates that formation of a CI dominates, and the observed trend in yield of the SOZ's with RH is controlled by the competing loss reaction of CI with water (i.e. **R2**).

There are three other main product peaks at masses less than Sqe. These peaks correspond to C_{17}-trienal (*m/z* 248.2), C_{22}-tetraenal (*m/z* 316.3), and C_{27}-pentaenal (*m/z* 384.3). These carbonyl species appear under dry conditions, and increasing the RH doubles their intensity. This can be explained qualitatively as being due to the CI + H_2O reaction that inhibits SOZ formation.

Carboxylic acids might be formed by the isomerization of p-CIs (**R4a**) with carbon numbers of 17 (*m/z*= 264.4), 22 (*m/z*= 332.5), and 27 (*m/z*= 400.6). There are peaks in the mass spectra consistent with these products, although at very low intensity. As found in previous studies, these peaks decrease with increasing RH.[6] The C_4 species levulinic and succinic acid, formed from sequential reactions of Sqe with ozone, were recently identified as main products in a monolayer study.[6] These products cannot be definitively observed here; if present the peaks are small and appear in a congested region of the mass spectrum. The lack of strong carboxylic acid signals is consistent with product trends with RH that suggest only s-CI is formed in significant quantities. It should be noted, however, that the differences in measured acid concentration between this and previous studies may originate from the different ionization sources used, since DART mass

spectrometry, employed by Zhou *et al.*[6], is known to have very high ionization sensitivity towards acids.

Typical products from OH reactions, such as alcohols,[44] are not observed. This suggests that under our reaction conditions OH formation from the 1,4 H-shift, observed in the gas phase, is a minor pathway, and therefore is not included in the simulations. However, it may be important under typical indoor air conditions where chemistry can occur over longer timescales and at lower [O_3], which can alter the relative importance of unimolecular vs. bimolecular pathways.

While the reactive decay of Sqe is observed to be independent of RH (Figure 2a), the SOZ, C_{27} aldehyde products and aerosol diameter exhibit a substantial dependence on water (Figure 4). At low RH (3%) there is a minimal loss of mass from the aerosol, resulting in shrinking of its diameter by 5%. As the RH is increased to 60% the diameter is observed to decrease by ~30%, indicating the formation of substantial quantities of gas phase reaction products. This decrease in aerosol diameter with RH is accompanied by similar decreases in the quantity of the particle phase C_{30} SOZ and C_{27} aldehyde products. When RH increases from 3 to 60%, the aldehyde increases by about 3x. The C_{30} SOZ exhibits the opposite behavior, a ~3x reduction in intensity occurs on going from RH = 3% to 60%. Together these observations show that there are substantial changes in the multiphase ozonolysis products of squalene driven mainly by the water content in the reactor. Lower molecular weight carbonyls form under wet conditions and the higher mass forms SOZ under dry conditions.

Simulation results are compared to experiment in Figure 4. Overall, the agreement for C_{27} formation and decay and particle size changes in Figures 4a and 4b is reasonable. The model predicted intensities of 30% SOZ and 70% carbonyls at 30% RH (Figure S7) are reasonable within experimental uncertainty, compared to recent velocity map imaging experiments, which measured

values of 15% and 85%, respectively.[20] It is clear from Figure 4c, however, that the simulation does not predict the relative humidity dependence of C_{30} SOZ formation above an RH of 3%, indicating that the mechanism is incomplete.

Several previous studies have examined the lifetime of Sqe in the presence of O_3 under a variety of conditions.[6, 19, 20, 22, 23, 32] These studies report a wide range of uptake coefficients, that depend on experimental conditions (e.g. RH, concentration and phase state of Sqe, etc.). In light of our results, measured uptake coefficients are an aggregate of two elementary steps (adsorption and reaction). The adsorption rate is controlled by site concentration, collision frequency and sticking probability. The adsorption site density will vary from experiment to experiment depending on, for example, whether bulk liquid, dispersed droplets on a support, or a thin uniform film is used. Thus one could imagine determining uptake coefficients in two very different kinetic regimes where: 1) O_3 adsorption *is not* the limiting step, i.e. the reaction is relatively slow, and 2) where O_3 adsorption *is* limiting due to low [O_3] or adsorption sites or both. The applicable kinetic regime for the experiment will determine the overall consumption rate of Sqe and hence the uptake coefficient. Furthermore, the substantial change in aerosol size under wet conditions can complicate the determination of uptake coefficients, which scale as the inverse square of the diameter.

Branching Ratio Primary vs. Secondary CI. As described above, the pattern of SOZ's observed in the experiment is consistent with forming mainly p-CI or s-CI rather than the gas phase POZ decomposition branching ratio (BR) of p-CI:s-CI = 53.5:46.5.[45] Using this gas phase branching ratio would produce a much larger array of possible SOZ as shown in Table S2 and Figure S5. For example, equal quantities of p- and s-CI should produce significant numbers of C_{21}, C_{39}, C_{44}, C_{49}, and C_{54} SOZ products (see Table S2), which are not observed in the experiment.

Based on these experimental findings we performed simulations to test sensitivities to two different BRs for p- and s-CI formation (Figure 5). The solid lines are for a BR of p-CI:s-CI = 10:90, which provides the best description of the experimental results. The dashed lines are for a BR of p-CI:s-CI = 50:50. It is clear that there is too much mass loss from the aerosol when p- and s-CI are formed with equal probability. In addition the aerosol size exhibits only a very weak RH dependence with the 50:50 assumption, which is inconsistent with observation. *Why* the selectivity in condensed phase is so different from that found in the gas phase is not clear; this finding would benefit from further theoretical and experimental investigations.

The enhanced mass loss from the aerosol predicted when significant quantities of p-CI are formed is due to the evaporation of the small ketone (C_3, C_8, C_{13}) co-product. Since this step doesn't involve water, rapid chemical erosion via p-CI formation would be predicted even under dry conditions. Although the reaction of the p-CI with water (**R2**) will form the observed C_{27}, C_{22}, and C_{17} aldehydes, these species do not exhibit the sensitivity to RH that is observed in the experiment (Figure 5b). Thus the weak RH dependence observed in the 50:50 scenario originates solely from reactions involving s-CI.

The simulations that are most consistent with experiment indicate that s-CI are formed at least 10 times faster than p-CI. This means that the most important CI's for squalene ozonolysis have small carbon numbers: C_3, C_8, and C_{13}. According to **R1**, the corresponding coproducts of these s-CI are the C_{27}, C_{22}, and C_{17} aldehydes. These are the main aldehydes observed in the experiment and they are present even under dry conditions since they originate directly from the POZ decomposition. As the RH is raised, the reaction rate of C_3, C_8, and C_{13} s-CI with water (**R2**) increases, forming the C_3, C_8, and C_{13} ketones, which are volatile and evaporate from the aerosol. This explains the experimental observation that chemical erosion of the aerosol depends upon

water. This scenario also accounts for the changes in product distribution as a function of RH. At low RH, the C_3, C_8, and C_{13} s-CI mainly react with C_{27}, C_{22}, and C_{17} aldehydes to form the observed distribution of C_{20}, C_{25}, C_{30}, C_{35}, C_{40} SOZ. At low RH, reaction with s-CI is the main sink for these aldehydes (i.e. via **R3**). As the RH is raised the s-CI no longer react only with the C_{27}, C_{22}, and C_{17} aldehydes but rather increasingly react with water (**R2**), which explains why the experimental observed product distributions shift from SOZ to aldehydes as the availability of water increases.

In summary, using the rate coefficients and branching ratios for p-CI:s-CI described above, the simulation can reproduce most of the experimental data. However, the loss of SOZ with increasing RH remains under-predicted. This suggests that there are missing sink reaction pathways for the SOZ not currently captured by **R1**-**R6**. We measured the hydrolysis rate of the SOZ's, and detected little if any reaction over time scale of the experiment (37s) (see Figure S8). Additional possibilities for the difference between simulated and experimental SOZ concentrations vs O_3 exposure include: 1) SOZ reactions with H_2O_2 formed in **R2** 2) other radical forming unimolecular decomposition pathways of SOZ[46] and 3) CI reactions with acids, which would indirectly control the quantity of SOZ formed. To improve the agreement between the experiment and the model, further work is needed to better understand the transformation chemistry of SOZ particularly under conditions that replicate indoor environments.

Implications for indoor air quality. In an indoor environment Sqe, which is one of the main organic contaminants present, has shown to be a major ozone sink and one of the main ozone scavengers on human surfaces.[5] The oxidation products influence air quality and occupant health, as they can act as skin and/or respiratory irritants. Gaining better mechanistic insight is therefore crucial for improving indoor air quality. Our study seeks to develop a detailed molecular-level understanding of the mechanistic pathways of the CI and their sensitivity to reaction conditions.

We found that the decomposition of the POZ predominantly leads to the formation of small secondary CI, which furthermore form ketones or isomerize to α-hydroxy ketones. α-hydroxy ketones have been found in indoor measurements of gas phase species to be among the major volatile primary products.[5] In a second generation ozonolysis step they can form dicarbonyl compounds, which are respiratory irritants[47] and may cause DNA damage.[48]

The formation of ketones is enhanced with increasing relative humidity and results in chemical erosion of the Sqe aerosol or surface. Under dry conditions the lifetime of a CI is about 7 s (Figure S9), whereas in the presence of water, CI instantly reacts to form reaction products with high volatility. Given the high concentration of Sqe, its ozonolysis products may make up a dominant part of indoor VOCs, particularly under humid conditions. If these are formed on the body envelope, the concentration of potentially harmful VOCs is increased by 1.2 to 2.5 times in our breathing zone compared to room levels.[5]

Our finding that the reaction of ozone occurs rapidly on the aerosol surface and therefore is transport limited may explain the wide range of reported uptake coefficients. Understanding how the ozone uptake to Sqe surfaces depends on varying conditions is particularly vital for improving comprehensive indoor air models, and predicting the proportions of gas phase and surface-bound products that may impact occupant health.

Supporting Information. The Supporting Information is available free of charge on the ACS Publications website at DOI:

Ozone adsorption kinetics; evaporation description; Mass, compound names, density and saturation vapor pressures of all modeled compounds; Model sensitivity tests for isomerization and evaporation; Bulk reaction model scenario; Primary CI and corresponding ketones; Secondary CI and corresponding aldehydes; SOZ formation

patterns; Total SOZ and Carbonyls; SOZ intensity under dry and humid conditions; Lifetime of CI.

Acknowledgments.

This work is supported by the Department of Energy, Office of Science, Office of Basic Energy Sciences, Chemical Sciences, Geosciences, and Biosciences Division, in the Gas Phase Chemical Physics Program under Contract No. DE-AC02-05CH11231. This research used the Advanced Light Source, which is a DOE Office of Science User Facility under contract no. DE-AC02-05CH11231. N.H. thanks the Alexander-von-Humboldt Foundation for a post-doctoral research fellowship. The authors thank Michael Jacobs (Lawrence Berkeley National Laboratory and UC Berkeley Department of Chemistry) for conducting the secondary ozonide hydrolysis measurements.

Corresponding Authors

Kevin R. Wilson, 510-495-2474, krwilson@lbl.gov

Frances A. Houle, 510-495-8135, fahoule@lbl.gov

Reference

1. Donahue, N. M.; Tischuk, J. E.; Marquis, B. J.; Huff Hartz, K. E., Secondary organic aerosol from limona ketone: insights into terpene ozonolysis via synthesis of key intermediates. *PCCP* **2007,** *9* (23), 2991.
2. Presto, A. A.; Huff Hartz, K. E.; Donahue, N. M., Secondary Organic Aerosol Production from Terpene Ozonolysis. 1. Effect of UV Radiation. *Environ. Sci. Technol.* **2005,** *39* (18), 7036.
3. Weschler, C. J., Roles of the human occupant in indoor chemistry. *Indoor Air* **2016,** *26* (1), 6.
4. Weschler, C. J., Ozone in Indoor Environments: Concentration and Chemistry. *Indoor Air* **2000,** *10* (4), 269.
5. Wisthaler, A.; Weschler, C. J., Reactions of ozone with human skin lipids: sources of carbonyls, dicarbonyls, and hydroxycarbonyls in indoor air. *Proc. Natl. Acad. Sci. U. S. A.* **2010,** *107* (15), 6568.
6. Zhou, S.; Forbes, M. W.; Abbatt, J. P. D., Kinetics and Products from Heterogeneous Oxidation of Squalene with Ozone. *Environ. Sci. Technol.* **2016,** *50* (21), 11688.

7. Morrison, G., Recent Advances in Indoor Chemistry. *Current Sustainable/Renewable Energy Reports* **2015,** *2* (2), 33.
8. Klepeis, N. E.; Nelson, W. C.; Ott, W. R.; Robinson, J. P.; Tsang, A. M.; Switzer, P.; Behar, J. V.; Hern, S. C.; Engelmann, W. H., The National Human Activity Pattern Survey (NHAPS): a resource for assessing exposure to environmental pollutants. *J. Expo. Anal. Environ. Epidemiol.* **2001,** *11* (3), 231.
9. Weschler, C. J.; Shields, H. C., Potential reactions among indoor pollutants. *Atmos. Environ.* **1997,** *31* (21), 3487.
10. Gómez Alvarez, E.; Amedro, D.; Afif, C.; Gligorovski, S.; Schoemaecker, C.; Fittschen, C.; Doussin, J.-F.; Wortham, H., Unexpectedly high indoor hydroxyl radical concentrations associated with nitrous acid. *Proc. Natl. Acad. Sci. U.S.A.* **2013,** *110* (33), 13294.
11. Weschler, C. J.; Shields, H. C., Production of the Hydroxyl Radical in Indoor Air. *Environ. Sci. Technol.* **1996,** *30* (11), 3250.
12. Milstone, L. M., Epidermal desquamation. *J. Dermatol. Sci.* **2004,** *36* (3), 131.
13. Picardo, M.; Ottaviani, M.; Camera, E.; Mastrofrancesco, A., Sebaceous gland lipids. *Dermato-endocrinology* **2009,** *1* (2), 68.
14. Coleman, B. K.; Destaillats, H.; Hodgson, A. T.; Nazaroff, W. W., Ozone consumption and volatile byproduct formation from surface reactions with aircraft cabin materials and clothing fabrics. *Atmos. Environ.* **2008,** *42* (4), 642.
15. Liu, S.; Thompson, S. L.; Stark, H.; Ziemann, P. J.; Jimenez, J. L., Gas-Phase Carboxylic Acids in a University Classroom: Abundance, Variability, and Sources. *Environ. Sci. Technol.* **2017,** *51* (10), 5454.
16. Fadeyi, M. O.; Weschler, C. J.; Tham, K. W.; Wu, W. Y.; Sultan, Z. M., Impact of human presence on secondary organic aerosols derived from ozone-initiated chemistry in a simulated office environment. *Environ. Sci. Technol.* **2013,** *47* (8), 3933.
17. Lakey, P. S. J.; Wisthaler, A.; Berkemeier, T.; Mikoviny, T.; Pöschl, U.; Shiraiwa, M., Chemical kinetics of multiphase reactions between ozone and human skin lipids: Implications for indoor air quality and health effects. *Indoor Air* **2016,** *27* (4), 816.
18. Kalogeropoulos, N.; Andrikopoulos, N. K., Squalene in oils and fats from domestic and commercial fryings of potatoes. *Int. J. Food Sci. Nutr.* **2004,** *55* (2), 125.
19. Lee, L.; Wilson, K., The Reactive–Diffusive Length of OH and Ozone in Model Organic Aerosols. *J. Phys. Chem. A* **2016,** *120* (34), 6800.
20. Jacobs, M. I.; Xu, B.; Kostko, O.; Heine, N.; Ahmed, M.; Wilson, K. R., Probing the Heterogeneous Ozonolysis of Squalene Nanoparticles by Photoemission. *J. Phys. Chem. A* **2016,** *120* (43), 8645.
21. Petrick, L.; Dubowski, Y., Heterogeneous oxidation of squalene film by ozone under various indoor conditions. *Indoor Air* **2009,** *19* (5), 381.
22. Wells, J.; Morrison, G.; Coleman, B., Kinetics and Reaction Products of Ozone and Surface-Bound Squalene. *J. ASTM Int.* **2008,** *5* (7), 12.
23. Fu, D.; Leng, C.; Kelley, J.; Zeng, G.; Zhang, Y.; Liu, Y., ATR-IR study of ozone initiated heterogeneous oxidation of squalene in an indoor environment. *Environ. Sci. Technol.* **2013,** *47* (18), 10611.
24. Smith, J. D.; Kroll, J. H.; Cappa, C. D.; Che, D. L.; Liu, C. L.; Ahmed, M.; Leone, S. R.; Worsnop, D. R.; Wilson, K. R., The heterogeneous reaction of hydroxyl radicals with sub-micron squalane particles: a model system for understanding the oxidative aging of ambient aerosols. *Atmos. Chem. Phys.* **2009,** *9* (9), 3209.

25. Gloaguen, E.; Mysak, E. R.; Leone, S. R.; Ahmed, M.; Wilson, K. R., Investigating the chemical composition of mixed organic–inorganic particles by "soft" vacuum ultraviolet photoionization: The reaction of ozone with anthracene on sodium chloride particles. *Int. J. Mass spectrom.* **2006,** *258* (1–3), 74.
26. Hinsberg, W. D., Houle, F. A. Kinetiscope a stochastic kinetics simulator. Available under a no-cost license from www.hinsberg.net/kinetiscope.
27. Wiegel, A. A.; Wilson, K. R.; Hinsberg, W. D.; Houle, F. A., Stochastic methods for aerosol chemistry: a compact molecular description of functionalization and fragmentation in the heterogeneous oxidation of squalane aerosol by OH radicals. *Phys. Chem. Chem. Phys.* **2015,** *17* (6), 4398.
28. Richards-Henderson, N. K.; Goldstein, A. H.; Wilson, K. R., Sulfur Dioxide Accelerates the Heterogeneous Oxidation Rate of Organic Aerosol by Hydroxyl Radicals. *Environ. Sci. Technol.* **2016,** *50* (7), 3554.
29. Liu, M. J.; Wiegel, A. A.; Wilson, K. R.; Houle, F. A., Aerosol Fragmentation Driven by Coupling of Acid-Base and Free Radical Chemistry in the Heterogeneous Oxidation of Aqueous Citric Acid by OH Radicals. *J. Phys. Chem. A* **2017,** *121* (31), 5856.
30. Houle, F. A.; Hinsberg, W. D.; Wilson, K. R., Oxidation of a model alkane aerosol by OH radical: the emergent nature of reactive uptake. *PCCP* **2015,** *17* (6), 4412.
31. Fendel, W.; Matter, D.; Burtscher, H.; Schmidt-Ott, A., Interaction between carbon or iron aerosol particles and ozone. *Atmos. Environ.* **1995,** *29* (9), 967.
32. Petrick, L.; Dubowski, Y., Heterogeneous oxidation of squalene film by ozone under various indoor conditions. *Indoor Air* **2009,** *19* (5), 381.
33. Taatjes, C. A.; Welz, O.; Eskola, A. J.; Savee, J. D.; Scheer, A. M.; Shallcross, D. E.; Rotavera, B.; Lee, E. P. F.; Dyke, J. M.; Mok, D. K. W.; Osborn, D. L.; Percival, C. J., Direct Measurements of Conformer-Dependent Reactivity of the Criegee Intermediate CH3CHOO. *Science* **2013,** *340* (6129), 177.
34. Taatjes, C. A.; Welz, O.; Eskola, A. J.; Savee, J. D.; Osborn, D. L.; Lee, E. P. F.; Dyke, J. M.; Mok, D. W. K.; Shallcross, D. E.; Percival, C. J., Direct measurement of Criegee intermediate (CH2OO) reactions with acetone, acetaldehyde, and hexafluoroacetone. *PCCP* **2012,** *14* (30), 10391.
35. Pryor, W. A.; Smith, K., Reactions of Radicals.25. Viscosity Dependence on Bond Homolysis - A Qalitative and Semiquantitative Test for Cage Return. *J. Am. Chem. Soc.* **1970,** *92* (18), 5403.
36. Vereecken, L.; Harder, H.; Novelli, A., The reactions of Criegee intermediates with alkenes, ozone, and carbonyl oxides. *PCCP* **2014,** *16* (9), 4039.
37. Berndt, T.; Jokinen, T.; Mauldin, R. L.; Petäjä, T.; Herrmann, H.; Junninen, H.; Paasonen, P.; Worsnop, D. R.; Sipilä, M., Gas-Phase Ozonolysis of Selected Olefins: The Yield of Stabilized Criegee Intermediate and the Reactivity toward SO2. *J. Phys. Chem. Lett.* **2012,** *3* (19), 2892.
38. Chhantyal-Pun, R.; Welz, O.; Savee, J. D.; Eskola, A. J.; Lee, E. P. F.; Blacker, L.; Hill, H. R.; Ashcroft, M.; Khan, M. A. H.; Lloyd-Jones, G. C.; Evans, L.; Rotavera, B.; Huang, H.; Osborn, D. L.; Mok, D. K. W.; Dyke, J. M.; Shallcross, D. E.; Percival, C. J.; Orr-Ewing, A. J.; Taatjes, C. A., Direct Measurements of Unimolecular and Bimolecular Reaction Kinetics of the Criegee Intermediate (CH3)2COO. *J. Phys. Chem. A* **2017,** *121* (1), 4.
39. Kurtén, T.; Rissanen, M. P.; Mackeprang, K.; Thornton, J. A.; Hyttinen, N.; Jørgensen, S.; Ehn, M.; Kjaergaard, H. G., Computational Study of Hydrogen Shifts and Ring-Opening Mechanisms in α-Pinene Ozonolysis Products. *J. Phys. Chem. A* **2015,** *119* (46), 11366.

538 40. Wiegel, A. A.; Liu, M. J.; Hinsberg, W. D.; Wilson, K. R.; Houle, F. A., Diffusive
539 confinement of free radical intermediates in the OH radical oxidation of semisolid aerosols. *PCCP*
540 **2017,** *19* (9), 6814.
541 41. Rembaum, A.; Szwarc, M., O-O Bond Dissociation Energies in Propionyl and Butyryl
542 Peroxides. *J. Chem. Phys.* **1955,** *23* (5), 909.
543 42. Compernolle, S.; Ceulemans, K.; Müller, J. F., EVAPORATION: a new vapour pressure
544 estimation methodfor organic molecules including non-additivity and intramolecular interactions.
545 *Atmos. Chem. Phys.* **2011,** *11* (18), 9431.
546 43. Razumovskii, S. D.; Lisitsyn, D. M., Reactions of ozone with double bonds in polymer and
547 biosystem chemistry. *Polymer Science Series A* **2008,** *50* (12), 1187.
548 44. Nah, T.; Zhang, H.; Worton, D. R.; Ruehl, C. R.; Kirk, B. B.; Goldstein, A. H.; Leone, S.
549 R.; Wilson, K. R., Isomeric product detection in the heterogeneous reaction of hydroxyl radicals
550 with aerosol composed of branched and linear unsaturated organic molecules. *J. Phys. Chem. A*
551 **2014,** *118* (49), 11555.
552 45. Richters, S.; Herrmann, H.; Berndt, T., Different Pathways of the Formation of Highly
553 Oxidized Multifunctional Organic Compounds (HOMs) from the Gas-Phase Ozonolysis of β-
554 Caryophyllene. *Atmospheric Chemistry and Physics Discussions* **2016,** *16*, 1.
555 46. Ellis, S. R.; Pham, H. T.; in het Panhuis, M.; Trevitt, A. J.; Mitchell, T. W.; Blanksby, S.
556 J., Radical Generation from the Gas-Phase Activation of Ionized Lipid Ozonides. *J. Am. Soc. Mass.*
557 *Spectrom.* **2017,** *28* (7), 1345.
558 47. Anderson, S. E.; Wells, J. R.; Fedorowicz, A.; Butterworth, L. F.; Meade, B. J.; Munson,
559 A. E., Evaluation of the Contact and Respiratory Sensitization Potential of Volatile Organic
560 Compounds Generated by Simulated Indoor Air Chemistry. *Toxicol. Sci.* **2007,** *97* (2), 355.
561 48. Roberts, M. J.; Wondrak, G. T.; Laurean, D. C.; Jacobson, M. K.; Jacobson, E. L., DNA
562 damage by carbonyl stress in human skin cells. *Mutation Research/Fundamental and Molecular*
563 *Mechanisms of Mutagenesis* **2003,** *522* (1–2), 45.
564 49. Kirschenbaum, L. J.; Rueckberg, B., A Correlation of the Solubility of Water in
565 Hydrocarbons as a Function of Temperature Based on the Corresponding Vapor Pressure of Pure
566 Water. *Chem. Sci. J.* **2013,** *2013* (CSJ-101), 1.

567 **Figure Captions**

568 **Figure 1.** Generalized reaction scheme for the oxidation of unsaturated hydrocarbons by O_3.

569 **Figure 2.** a) Reactive decay of 300 nm size-selected Sqe aerosol (inferred from the intensity of the
570 peak at *m/z* 410.39) for RH = 3, 20, 40 and 60% with simulation results; b) simulated reactive
571 decay for two different *k* scenarios compared to experimental decay of Sqe (see Supplemental
572 Information); c) Comparison of measured (filled red points) and simulated (green and blue circles,
573 dashed lines) results, which evaluate sensitivity of the Sqe + O_3 rate coefficient. Red corresponds

574 to $k_1 = 1.25 \cdot 10^{-15}$ cm^3 s^{-1}, green to $k_2 = 1.21 \cdot 10^{-13}$ cm^3 s^{-1}.[19, 43] Error bars in a and b are the standard
575 deviation of the measured ion signal about its average.

576 **Figure 3.** 10.2 eV photoionization mass spectra recorded for polydisperse Sqe aerosol at a) RH =
577 3, b) 30 and c) 60%. For clarity only normalized difference MS are displayed, original spectra are
578 shown in the SI (Figure S4).

579 **Figure 4.** Overlay of experimental measurements of 300 nm size-selected Sqe aerosol, after
580 reactive uptake of ozone at different RH (3% to 60%), with simulation results. The same trends
581 are observed for all measured particle diameters and polydispers aerosol (SI). a) Change of particle
582 diameter; b) kinetic evolution of the secondary ozonide with the highest abundancy (*m/z* 458.38);
583 c) kinetic evolution of C27 pentaenal (*m/z* 384.34). The error bars in a are estimated from the
584 SMPS bin width and replicate measurements. The error bars in b and c are estimated using the
585 standard deviation of the measured ion signal about its average.

586 **Figure 5.** Sensitivity test for different branching ratios of **R1**. Solid lines represent a 1:10
587 primary:secondary CI ratio, dashed lines are model results for a 1:1 ratio. a) Particle diameter
588 change as function of RH. b) Maximum intensity of C27 (blue triangles) and SOZ (green circles)
589 as function of RH.

590

591 Table 1. Reaction Scheme and Rate Constants for Stochastic Simulations.[a)]

No.	Reaction step	Rate constant	Notes
	O_3_gas → O_3_adsorbed	1.97 s^{-1}	b)
R1	Sqe + O_3 → s/p-CI + R=O	$1.25 \cdot 10^{-15}$ cm^3 $molec^{-1}$ s^{-1}	c),d)
R2	CI + H_2O → R=O + H_2O_2	5.14 s^{-1}	e)
R3	CI + R=O → SOZ	$6.7 \cdot 10^{-19}$, $1.3 \cdot 10^{-18}$ cm^3 $molec^{-1}$ s^{-1}	f)
R4	CI → R(O)OH, HOR=O	5 s^{-1}	Ref.[37]
R6	CI + O_3 → R=O	$4 \cdot 10^{-13}$ cm^3 $molec^{-1}$ s^{-1}	Ref.[36]

592 [a)] **R5** was not considered in the model (see text for details. [b)] Rate coefficient depends on particle diameter (*d*) and
593 average [O_3]; here: *d*=300 nm, [O_3]=$2.81 \cdot 10^{13}$ molecules cm^{-3}. [c)] Either a pair of aldehyde and secondary Criegee
594 intermediate (sCI) or ketone and primary CI (pCI) can be formed. See Computational Details and Results and
595 Discussion for details on branching ratios. [d)] Experimental second-order rate constant taken from Ref. [43]. [e)] Treated as
596 pseudo first order where [H_2O] = 3-60% (shown for 0%), $k = 1 \cdot 10^{-14}$ cm^3 $molecules^{-1}$ s^{-1} (from Ref. [33]) and the
597 dimensionless Henry's law constant is $2.6 \cdot 10^{-2}$, which applies to solubility of water in aliphatic compounds with
598 comparable viscosity.[49] [f)] Constrained by calculation and experiment, corrected for solvent-cage effects and optimized
599 to multiple experimental data sets (see text for details).
600

601

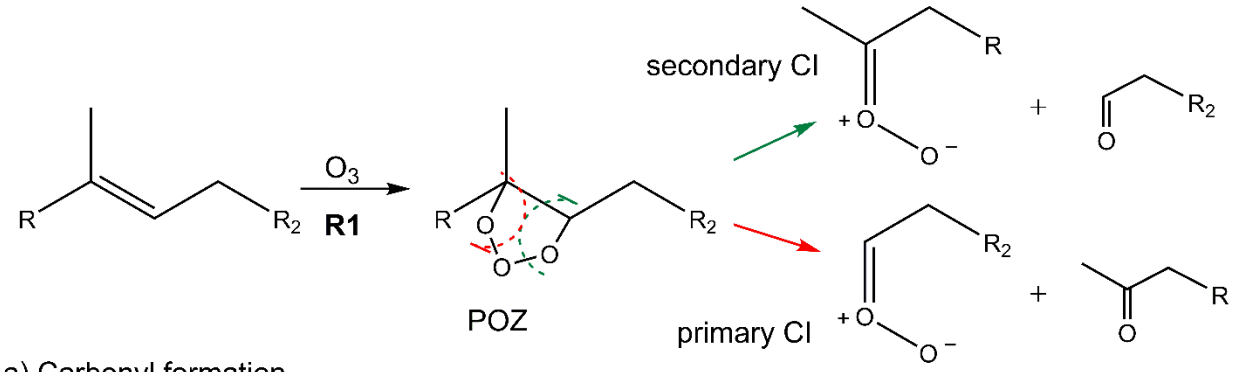

a) Carbonyl formation

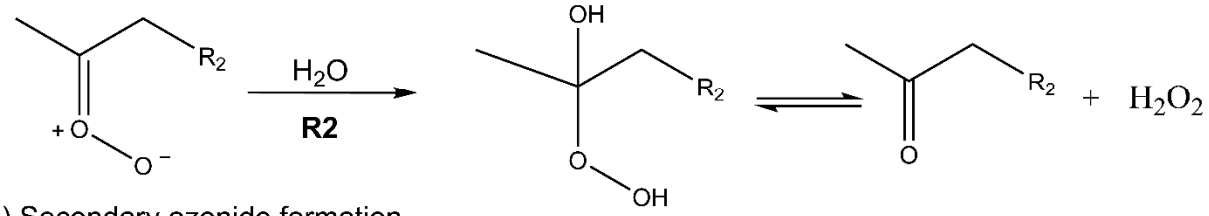

b) Secondary ozonide formation

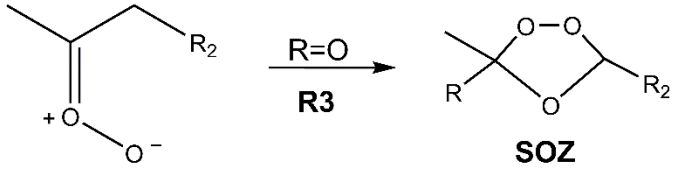

c) Rearrangements

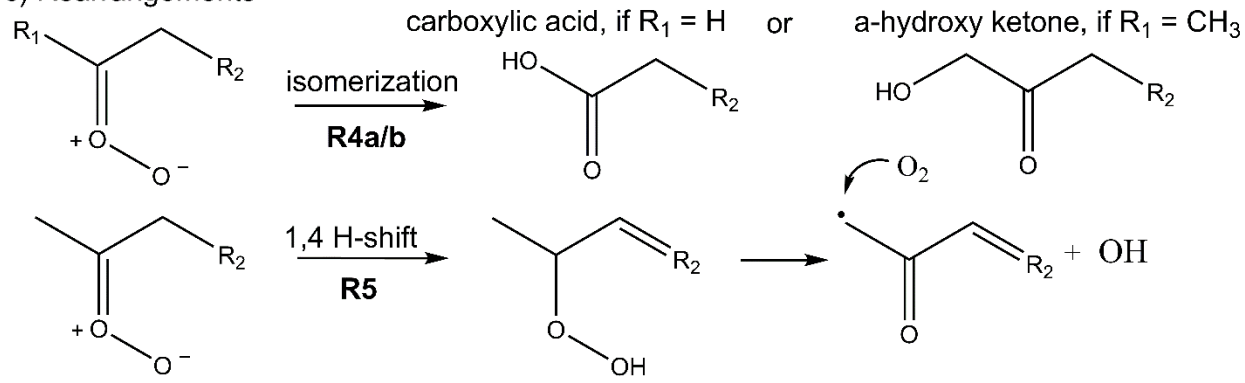

d) Carbonyl formation II

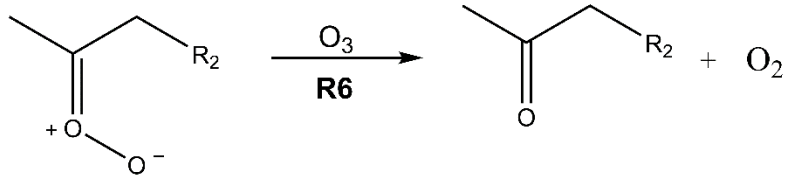

602

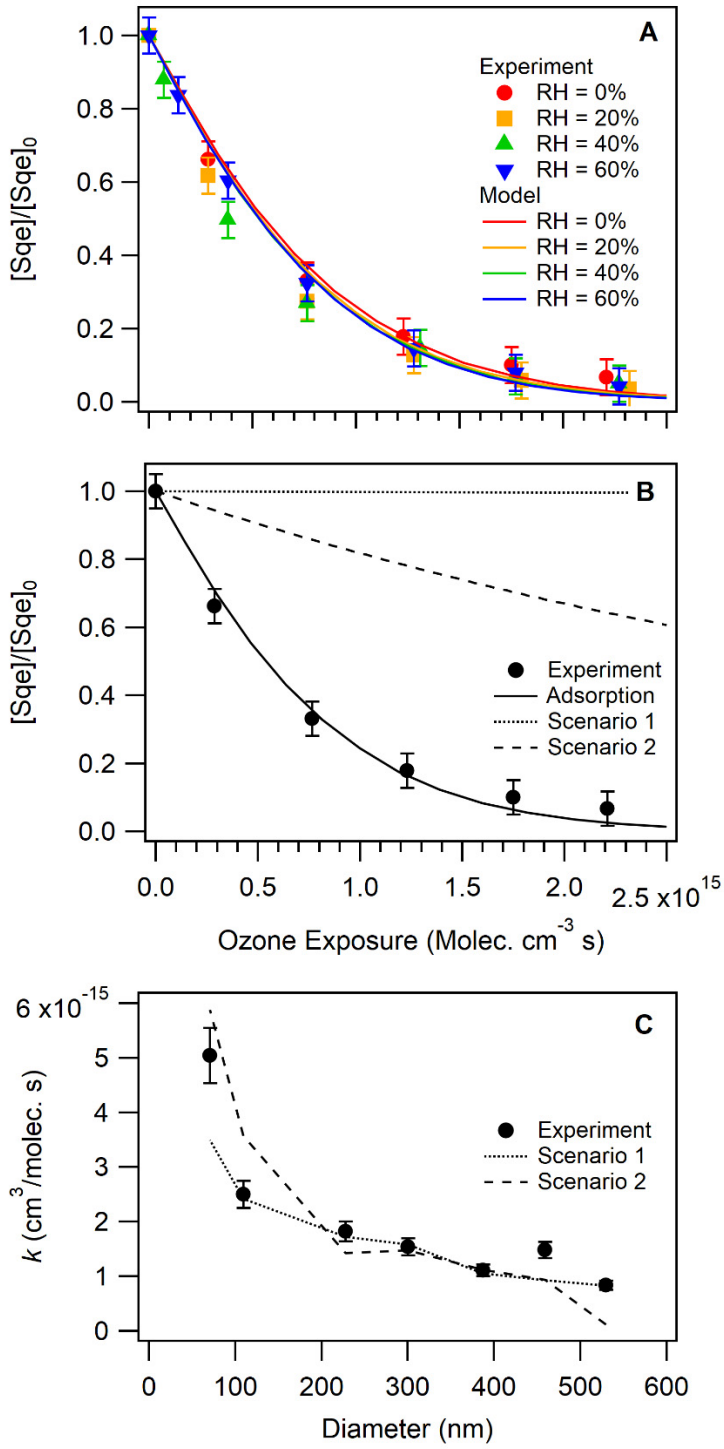

603

604 **Figure 2**

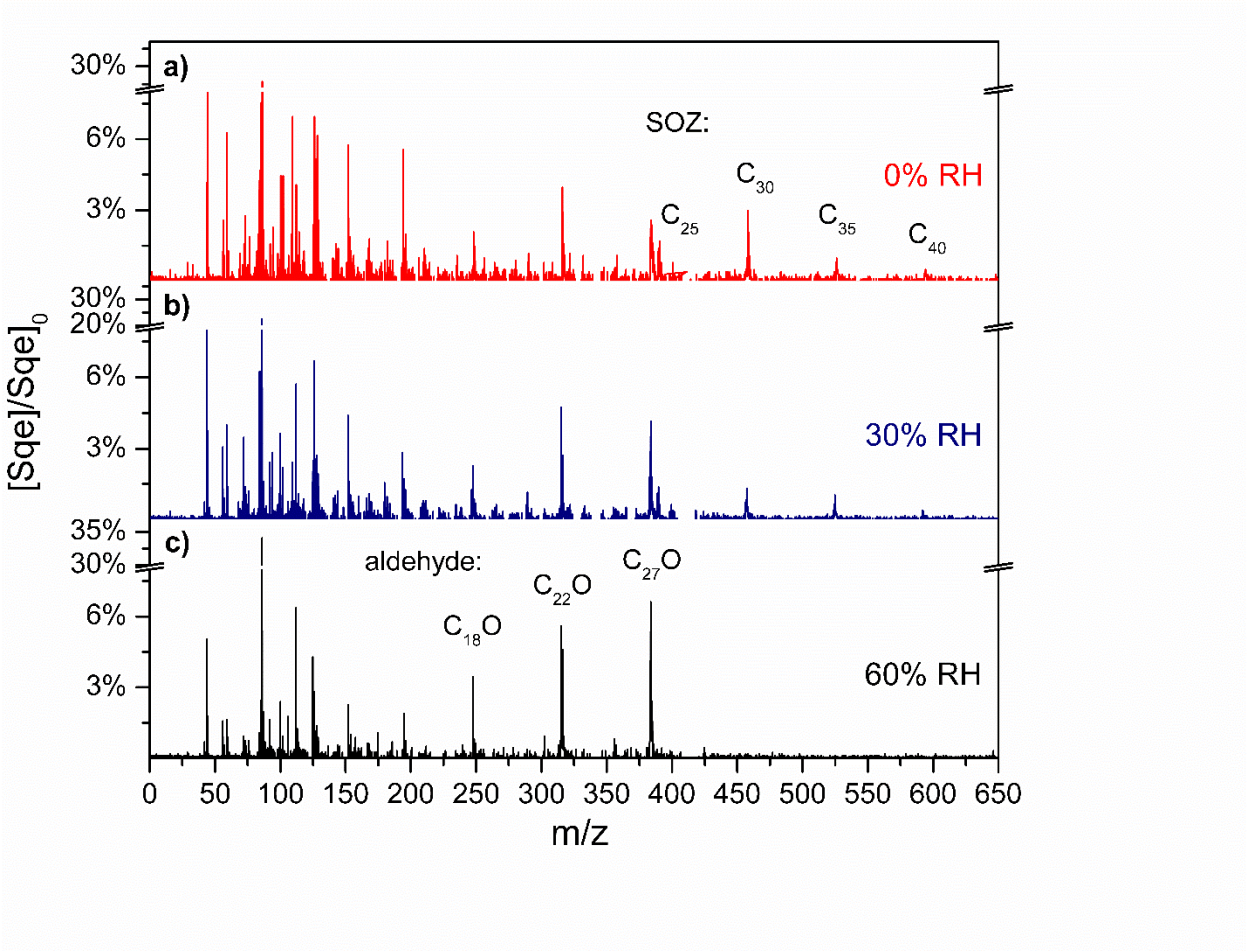
a)
SOZ:
0% RH
C25
C30
C35
C40
b)
30% RH
c)
aldehyde:
C18O
C22O
C27O
60% RH
[Sqe]/Sqe]0
m/z

Figure 3

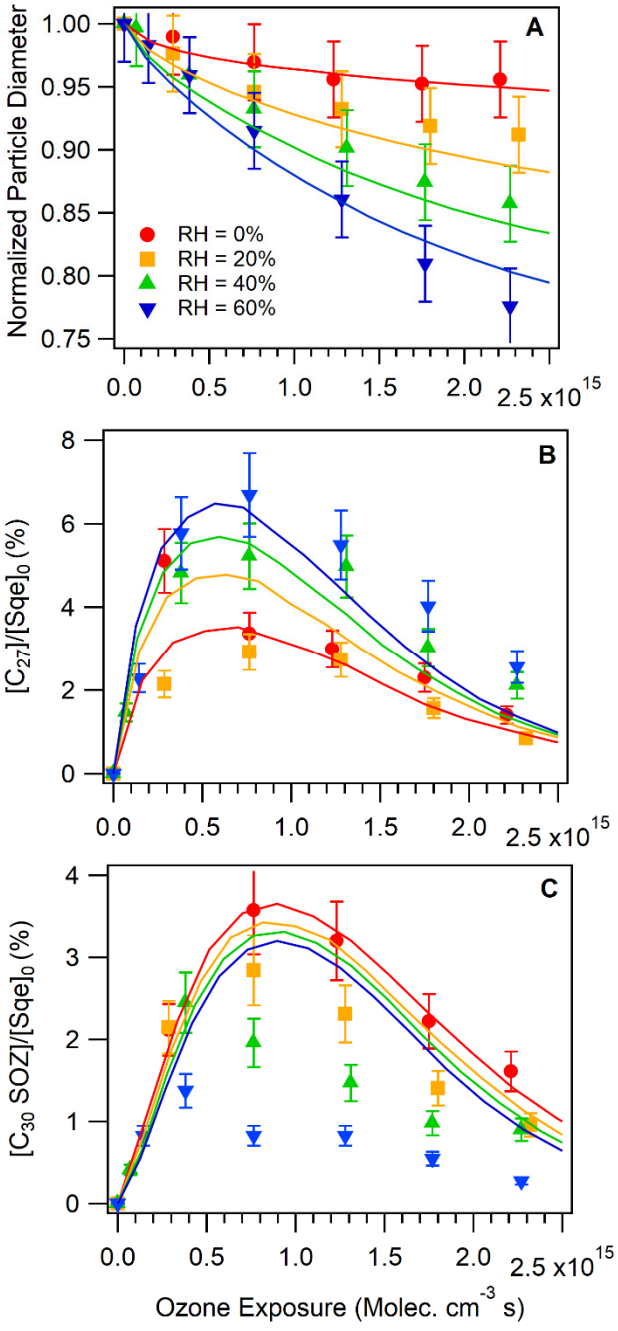
A
Normalized Particle Diameter
1.00
0.95
0.90
0.85
0.80
0.75
RH = 0%
RH = 20%
RH = 40%
RH = 60%
0.0
0.5
1.0
1.5
2.0
2.5 x10^15
B
[C27]/[Sqe]0 (%)
8
6
4
2
0
C
[C30 SOZ]/[Sqe]0 (%)
4
3
2
1
0
Ozone Exposure (Molec. cm^-3 s)

Figure 4

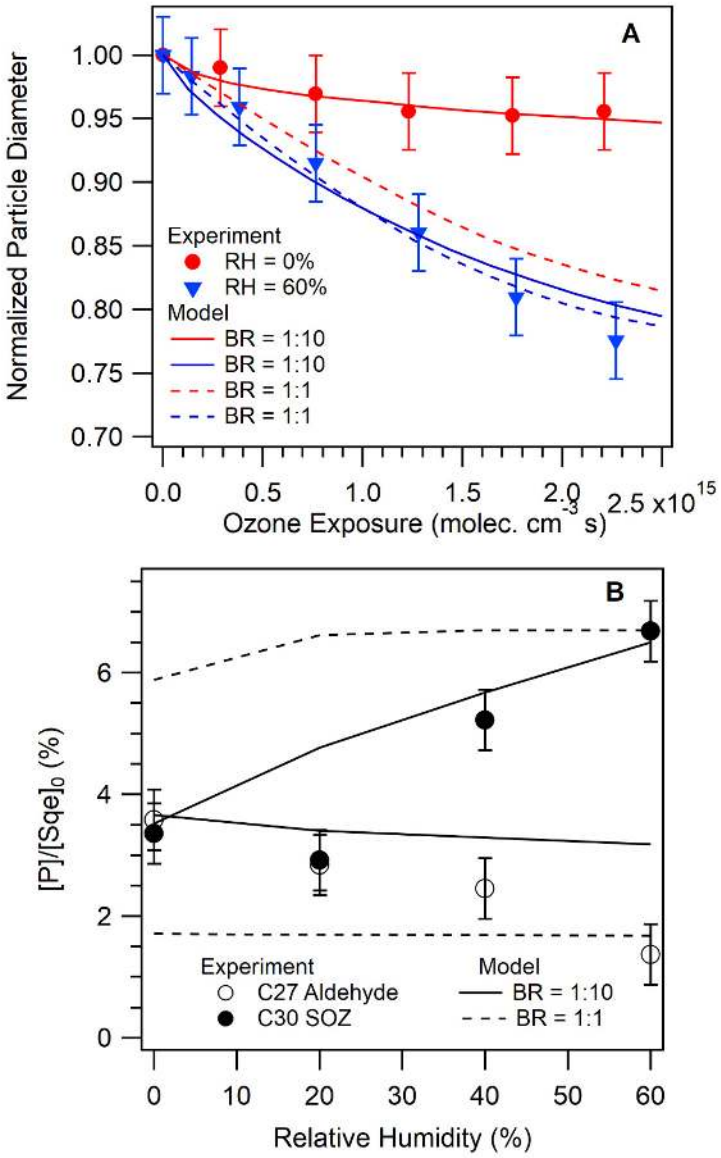
A
Normalized Particle Diameter
1.00
0.95
0.90
0.85
0.80
0.75
0.70
Experiment
RH = 0%
RH = 60%
Model
BR = 1:10
BR = 1:10
BR = 1:1
BR = 1:1
0.0
0.5
1.0
1.5
2.0
2.5 x10^15
Ozone Exposure (molec. cm^-3 s)
B
[P]/[Sqe]0 (%)
6
4
2
0
Experiment
C27 Aldehyde
C30 SOZ
Model
BR = 1:10
BR = 1:1
0
10
20
30
40
50
60
Relative Humidity (%)

Figure 5

644
645
646
647
648
649 Table of Contents Graphic
650

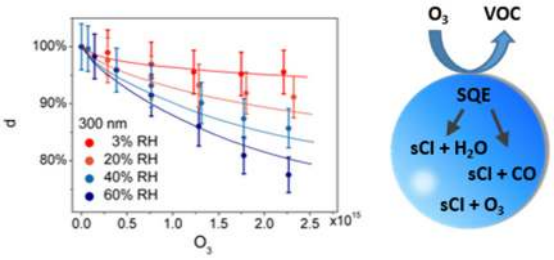

651